crystals

MDPI

Article

Computational Simulation by Phase Field: Martensite Transformation Kinetics and Variant Selection under External Fields

Chenchong Wang *, Jiahua Yuan and Minghao Huang

State Key Laboratory of Rolling and Automation, Northeastern University, Shenyang 110819, China; 2010213@stu.neu.edu.cn (J.Y.); 1710215@stu.neu.edu.cn (M.H.)
* Correspondence: wangchenchong@ral.neu.edu.cn; Tel.: +86-136-1404-2499

Abstract: Tailoring martensite transformation is critical for improving the mechanical properties of advanced steels. To provide preliminary guidance for the control of martensite transformation behaviour using external fields by computational simulation method, the phase-field method was used to calculate the morphology evolution, kinetics, and variant selection of the martensite transformation under different loading modes and magnetic field intensities. The incubation, transformation, and stable stages of the three variants based on the Bain strain group were investigated using different kinetic curves. These results clearly indicate that both uniaxial tension and compression can greatly promote the formation of martensite during the transformation stage and cause an obvious preferred variant selection. In contrast, the different variants have relatively balanced forms under shearing conditions. In addition, the magnetic field is a gentler way to form a state with balanced variants than other techniques such as shearing. Additionally, all these simulation results are consistent with classical martensitic transformation theory and thermodynamic mechanism, which proves the rationality of this research. The aim of the present study was to provide qualitative guidance for the selection of external fields for microstructural improvement in advanced steels.

Keywords: external field; phase field; phase transformation; simulation; transformation-induced plasticity

Citation: Wang, C.; Yuan, J.; Huang, M. Computational Simulation by Phase Field: Martensite Transformation Kinetics and Variant Selection under External Fields. *Crystals* **2022**, *12*, 829. https://doi.org/10.3390/cryst12060829

Academic Editors: Zhengzhi Zhao, Jun Hu and Pengfei Gao

Received: 23 May 2022
Accepted: 9 June 2022
Published: 11 June 2022

1. Introduction

The transformation-induced plasticity (TRIP) effect is the core mechanism for obtaining a good combination of strength and ductility [1–6] in materials such as advanced high-strength automotive steel [7–9] and cryogenic steels [10,11]. Therefore, to tailor martensite characteristics using special pretreatment during steel preparation or evaluate the performance of steels in different service environments, a deep understanding of martensite transformation behaviour under external fields, such as different stress–strain and electromagnetic fields, is of critical importance.

The effect of external fields on martensite transformation behaviour is a long-standing topic, which has a rich foundation in previous research, especially the effect of the stress–strain field [12–16]. Various studies have shown that many different factors of the loading process affect martensite transformation behaviour, including the stress value, loading temperature, strain rate, and loading mode. Different loading modes not only cause substantially different martensite transformation kinetics, but also affect the mechanism of nucleation, phase transformation sequence, and even variant selection [17–20]. First, many studies on kinetics have shown that deformation in the tension test leads to a higher amount of martensite transformation compared to that of the compression test [16,20]. In addition, most of these studies explain this phenomenon as due to the difference in nucleation rates. Tension and rolling can provide more active slip systems, leading to a higher number of shear band intersections for martensite nucleation [16]. In addition to

nucleation, Hyunmin Kim et al. [13] investigated the tension–compression asymmetry of martensitic transformation behaviour by conducting dynamic tensile and compressive tests in 2015. Their investigation clearly shows that the $\gamma \rightarrow \alpha'$ transformation sequence is inhibited by dynamic compressive loading because of the required additional molar volume expansion; similarly, the $\gamma \rightarrow \varepsilon \rightarrow \alpha'$ transformation sequence is probably promoted by tensile loading. In addition, the effect of the deformation mode on variant selection has also been analysed in several studies, but a more systematic approach is required for firm conclusions [12,14]. Except for the stress–strain field, the effect of the electromagnetic field on martensite transformation has been commonly studied using experimental methods to demonstrate its potential for tailoring martensite characteristics [21–23]. Recently, Yuan et al. [21] systematically analysed the effects of both magnetic fields and austenite grain sizes on martensitic transformation, including the martensite start temperature, kinetics, nucleation, transformation sequence, and variant selection.

Based on qualitative experimental results, simulation methods were also built for further quantitative guidance and predicting martensite transformation behaviour, especially kinetics and variant selection [24–32]. With the exception of various classical constitutive models such as the Olson–Cohen model [29,30], various studies on this topic have focused on the phase-field method because of its advantage in describing morphology evolution [27,28,31,32]. In 2000, Artemev et al. [27] simulated the effect of stress on martensite transformation using a phase-field model based on the strain energy functional. Although this preliminary attempt only focused on a single crystal system without considering the self-coordination effect during the transformation, their study provides an example of the quantitative analysis of martensite morphology evolution and variant selection using simulation. Subsequently, Malik et al. [28] explored this topic for polycrystalline iron-based alloys by coupling the micro-elastic and plastic deformation theories. A more functional phase-field model was built to further analyse the effect of the deformation mode, including uniaxial tensile, compressive, shear loading, and hydrostatic stresses. Recently, various further research has focused on the topic of martensite transformation simulation using the phase-field method and has reported exciting progress [33–35]. In Ahluwalia et al.'s work [33], both elastic and plastic effects were considered in a phase-field framework, and this helped to simulate the evolution of all the 24 transformation variants in high-carbon steel. In Basak et al.'s work [34], martensitic transformation induced by the matrix–precipitate interface was calculated using a thermodynamically consistent multiphase phase-field method. It can greatly help to tailor the cyclic martensitic transformations in shape memory and elastocaloric alloys. Additionally, in Kundin et al.'s work [35], an improved 3D microelastic-plastic phase-field model, which could be used to simulate a butterfly-type martensitic transformation in a Fe–30 wt % Ni alloy, was successfully established. All these recent works prove that the phase-field method is a vigorous method in the field of martensite transformation simulation. However, few studies have modelled the effect of the magnetic field on martensite transformation, and the phase-field models for the different loading modes mentioned above artificially set the initial nucleation conditions, which could partly affect the generality of the models.

In this study, a phase-field model was built to analyse the effect of different loading modes and magnetic fields on martensite transformation behaviour, including both kinetics and variant selection. This study provides a preliminary attempt to build models that guide the tailoring of martensite characteristics using different external fields.

2. Computational Scheme

In this research, the phase-field model was coded using the FORTRAN language and solved using Fourier transformation. The simulation was performed on a $128 \times 128 \times 1$ mesh after simulation space optimisation. The framework of the phase-field simulation in this

research is shown in Figure 1. The evolution equation for the martensitic transformation based on the three Bain strain groups in this study is expressed as Equation (1).

$$\frac{\partial \eta_i(r,t)}{\partial t} = -\sum_{i=1}^{3} L_{ij} \cdot \left(\frac{\delta G_{ch}}{\delta \eta_j} + \frac{\delta G_{el}}{\delta \eta_j} + \frac{\delta G_{grad}}{\delta \eta_j} \right), \quad (1)$$

where G_{ch}, G_{el}, and G_{grad} are the chemical Gibbs free, elastic, and interface energies, respectively, and L_{ij} represents the kinetic coefficient, which is considered isotropic.

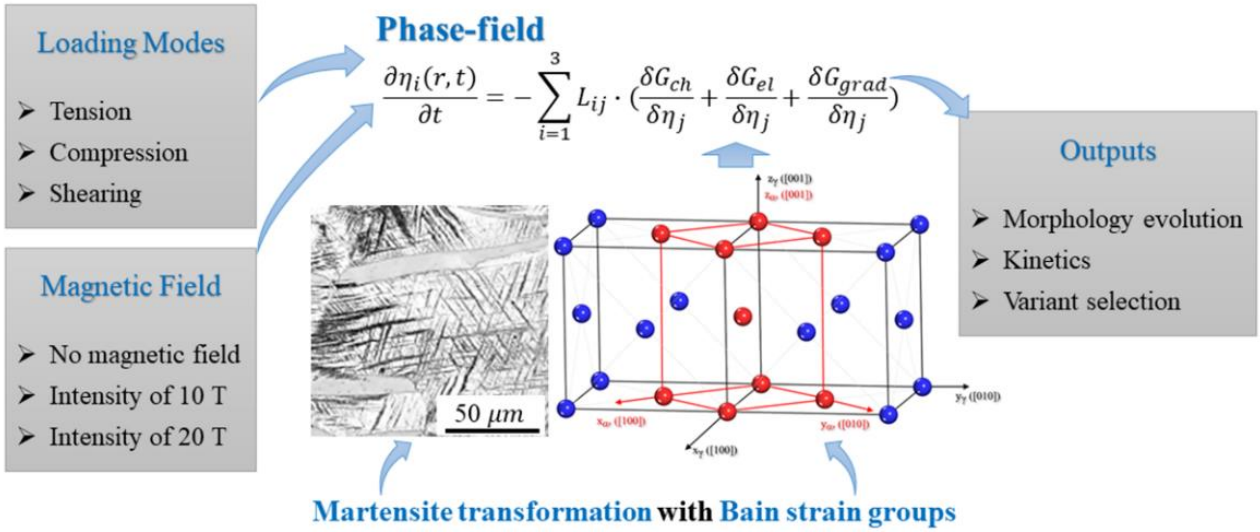

Figure 1. The framework of the phase-field simulation in this research.

The bulk energy difference between austenite and martensite represents the driving force. The Landau-type free energy equation was employed to describe the energy evolution of the martensitic transformation, which is a function of the relevant physical variables and temperature [36,37]:

$$G_{ch} = A_2 \left(\sum_{i=1}^{3} \eta_i^2 (\eta_i - 1)^2 \right) + A_{42} \sum_{i \neq j} \eta_i^2 \eta_j^2 + A_{62} \sum_{i \neq j = k} \eta_i^2 \eta_j^2 \eta_k^2 + \frac{T - T_0}{T_0} Q \cdot H(\{\eta_i\}), \quad (2)$$

where η_i, η_j, and η_k are the phase-field variables; A_2, A_{42}, and A_{62} are the Landau coefficients; T_0 is the temperature at which the Gibbs free energies between the austenite and transformed martensite are equal; and $H(\{\eta_i\})$ is the interpolation function:

$$H(\{\eta_i\}) = B \left(\sum_{i=1}^{3} \left(3\eta_i^2 - 2\eta_i^3 \right) \right), \quad (3)$$

where B is the interpolation function coefficient.

According to Khachaturyan's micro-elastic theory [27], the elastic strain energy generated during the phase transformation is expressed by Equation (4).

$$G_{el} = \frac{1}{2} C_{ijkl} \cdot \left(\varepsilon_{ij}^{\alpha} + \delta \varepsilon_{ij}^{el} - \varepsilon_{ij}^{0} \right) \cdot \left(\varepsilon_{kl}^{\alpha} + \delta \varepsilon_{kl}^{el} - \varepsilon_{kl}^{0} \right), \quad (4)$$

where C_{ijkl} is a fourth-order elastic modulus tensor, $\varepsilon_{ij}^{\alpha}$ and $\varepsilon_{kl}^{\alpha}$ are the strains applied by the external field to the system, $\delta \varepsilon_{ij}^{el}$ and $\delta \varepsilon_{kl}^{el}$ are the inhomogeneous elastic strain tensors, and ε_{ij}^{0} and ε_{kl}^{0} are the intrinsic strain tensors.

The interface between variants of martensite produce interfacial energy, owing to the irregular arrangement of the structures. The interface energy is expressed by Equation (5).

$$G_{grad} = \frac{1}{2}\sum_{p=1}^{3}\beta_{ij}(p)\frac{\partial\eta_p(r,t)}{\partial x_i}\frac{\partial\eta_p(r,t)}{\partial x_j}, \quad (5)$$

where β_{ij} is the interface gradient coefficient that is set as the isotropic interface property.

To simulate the magnetic field effect, another contribution term of the system free energy related to the saturation magnetisation was added to Equation (1). This magnetic energy, called G_{mag}, is expressed by Equation (6) [38]:

$$G_{mag} = -V_m\Delta M\mu_0 H, \quad (6)$$

where V_m is the molar volume of austenite, μ_0 is the vacuum permeability, H is the intensity of the external magnetic field [39], and ΔM is the saturation magnetisation difference between austenite and martensite; the saturation magnetisation value of the martensite phase is much higher than that of the austenite phase; thus, M_{Sat}^{MAR} is assumed to represent ΔM. The kinetic equations were solved in dimensionless units; thus, all the parameters were normalised, and parameters related to the characteristic energy were normalised by 10^{-9} J/mol [36]. The values of the key parameters used in the simulations are listed in Table 1 and Q* means the standard normalization value of Q.

Table 1. Values of the non-dimensional parameters in phase-field simulations.

Parameters	Values	Parameters	Values
A_2	0.1	Q*	0.35
A_{42}	5.0	V_m	6.8×10^{-6} m^3/mol
A_{62}	5.0	M_{Sat}^{MAR}	1.18×10^{6} Am^{-1}
T_0	429 K	μ_0	$4\pi \times 10^{-7}$ N/A^2

3. Results

This section is divided into subsections. A concise, precise description of the experimental results, their interpretation, and the experimental conclusions that can be drawn is provided.

3.1. Effect of the Loading Mode on Martensite Transformation Behaviour

The phase-field simulation starts with the austenite phase in a face-centred cubic (FCC) crystal structure. Random martensitic nucleation initiates the phase transformation, and, as a result, the parent phase with the FCC structure transforms into a new phase with a body-centred cubic crystal (BCC) structure. In reality, the FCC coherent transformation of the $\{111\}_\gamma$ plane leads to 24 different orientation variants. For simplicity, according to the crystallographic orientation relationship between FCC and BCC structures, the BCC structure is produced using three different deformations of the original FCC lattices. Thus, these different deformations are associated with three particular variants of the Bain strain. The three Bain variants are labelled by their deformation axes {xyz} [36,40].

In this study, different loading modes including uniaxial tension, uniaxial compression, and shearing were simulated. Figure 2 shows a qualitative comparison of the variant morphologies for the different loading modes. The white, blue, and pink phases represent variants 1, 2, and 3, respectively, of martensite. The black phase is austenite. As shown in Figure 2a, a multi-variant nucleation method was adopted in this simulation, and nine martensite nuclei were randomly created in the simulation domain. After 40 time steps, different variant selection trends are clearly shown in the different loading modes (Figure 2b–d). In particular, for uniaxial compression (Figure 2c), single variant 2 dominates compared to the others. Therefore, to perform an in-depth analysis of the variant selection behaviour, the kinetic curves for the three variants for different loading modes are plotted

in Figure 3. For all the different loading modes, the kinetic curves of variant 1 can be divided into three stages: incubation, transformation, and stable. As shown in Figure 3a, compression strain leads to a relatively shorter incubation stage than tension or shearing. In addition, uniaxial compression loading causes the highest growth rate of variant 1 in the transformation stage. In contrast, shearing significantly inhibits the rapid formation or growth of variant 1. Similar to the growth rate, uniaxial compression loading leads to the highest volume fraction of variant 1 after the final stable stage. However, tension and shearing lead to almost the same final volume fraction of variant 1, although the tension mode has a slightly higher growth rate than shearing.

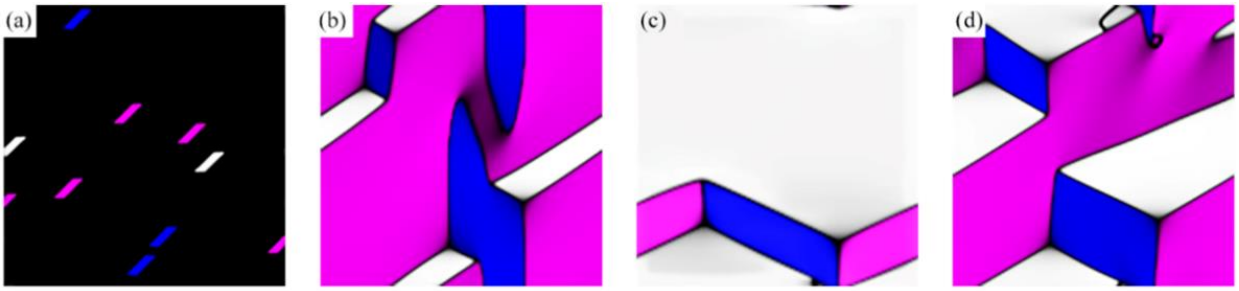

Figure 2. Comparison of variant morphology for different loading modes. (**a**) Random distribution of nucleation sites, (**b**) the final steady state for uniaxial tension, (**c**) the final steady state for uniaxial compression, and (**d**) the final steady state for shearing.

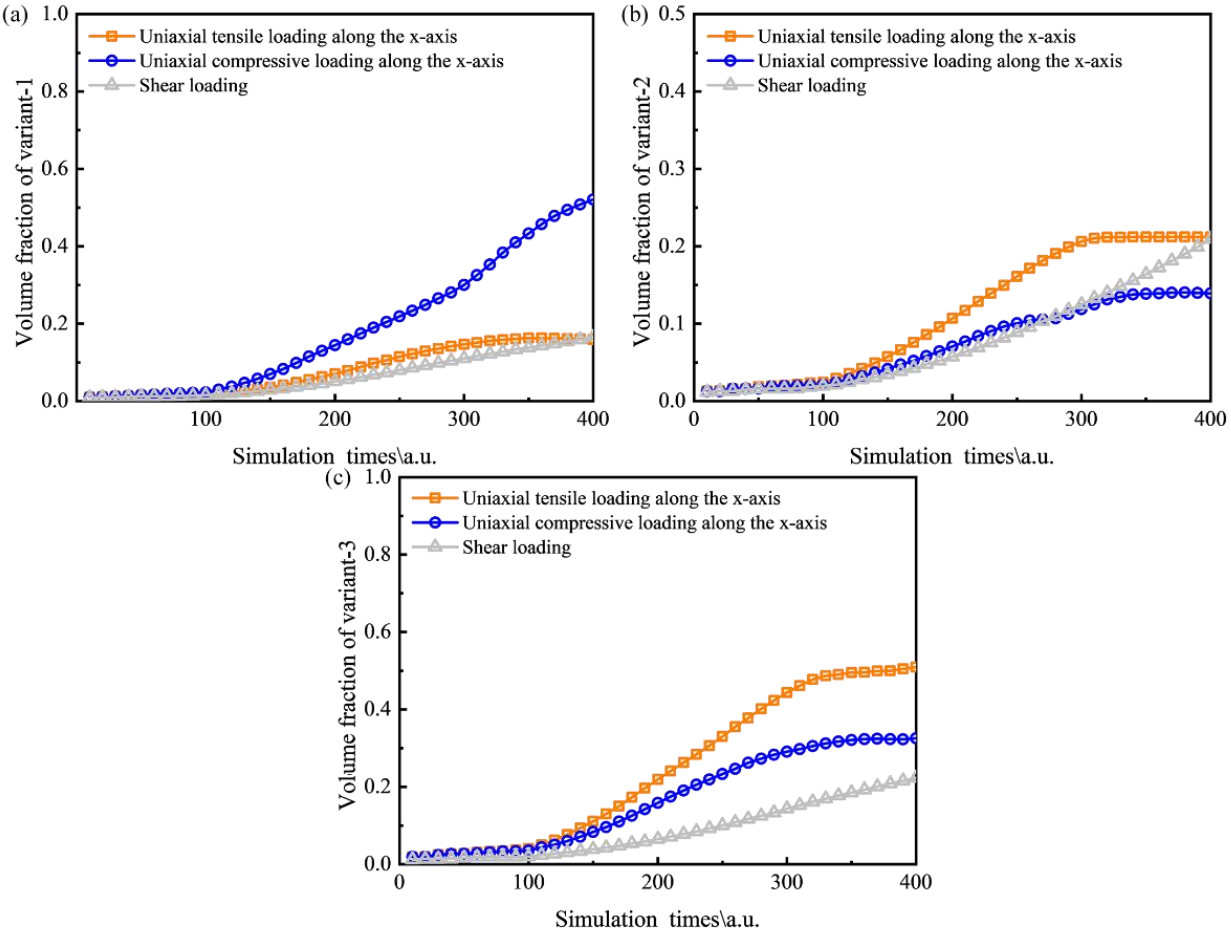

Figure 3. The kinetic curves of the three variants for different loading modes. (**a**) Variant 1, (**b**) variant 2, and (**c**) variant 3.

For further analysis, the relationship between the Bain strain group and austenite crystal coordinate system should be considered. Based on this relationship, the free strain of variant 1 has a negative strain along the *x*-axis. According to the theory of maximum principal stress, the shear deformation applied in the XZ direction forms a normal component stress along the *x*-axis direction. Therefore, the transformation of variant 1 is inhibited by this normal component stress. For uniaxial tension along the *x*-axis direction, the direction of the external stress is opposite to the strain direction of deformation. The system also tends to inhibit the transformation of variant 1 to balance the energies of the internal and external fields. For uniaxial compression along the *x*-axis, the direction of the external stress is the same as that of the strain. Therefore, the formation of variant 1 is promoted. Tsuchida et al. [41] explained these phenomena in their study. For uniaxial tension, the deformation strain is parallel to the tensile direction. Therefore, martensite grown in this direction has a lower nucleation barrier and is more prone to break the nucleation barrier and transform. In this situation, the variants in the other directions are inhibited. Similarly, for shearing and compression, the strain direction can also affect the nucleation barrier of the martensitic transformation, thereby affecting variant selection.

Figure 3b shows the kinetic curves of variant 2. For variant 2, all loading modes have nearly identical incubation stages. However, in the transformation stage, uniaxial tension shows a relatively higher growth rate than shearing or compression. In addition, the volume fraction of variant 2 for uniaxial tension is more stable than that for shearing or compression. Because the stress–strain condition of uniaxial compression is beneficial for the formation of variant 1, as mentioned above, the final volume fraction of variant 2 is only 1/5 that of variant 1 under uniaxial compression. Finally, Figure 3c shows the kinetic curves for variant 3. Similarly to variant 2, all the different loading modes have nearly the same incubation stages for variant 3. However, uniaxial tension loading causes a significantly higher growth rate of variant 3 in the transformation stage. In addition, the final volume fraction of variant 3 under uniaxial tension loading is the highest. The mechanism of this phenomenon is similar to that of variant 1 under uniaxial compression loading. For variant 3, under uniaxial tension loading, the direction of the external stress is the same as that of the strain, and this direction can help variant 3 break the nucleation barrier more easily. Therefore, variant 3 is preferred under uniaxial tension loading. In summary, because either uniaxial tension or compression has principal stress in a single direction, the preferred variant selection is formed in that direction. In contrast, for shearing that has a relatively balanced stress distribution in different directions, the preferred variant selection is insignificant.

In addition to the kinetic curves of every single variant, Figure 4 shows the kinetic curves of the martensite transformation for different loading modes. With the same loading stress, uniaxial tension and compression loading modes clearly lead to significantly higher martensite transformation rates than shearing loading does. Martensite transformation can cause volume expansion. The loading modes of uniaxial tension and compression can easily provide free space for this type of volume expansion. In addition, the stress conditions for uniaxial tension and compression benefit the formation of some variants, as previously mentioned. Therefore, martensitic transformation is greatly promoted under uniaxial tension and compression. However, regardless of the external stress conditions, all three variants nucleate and grow further instead of being eliminated. During the transformation process, the system balances the energy of the internal and external fields to promote or inhibit the formation of relevant variants, but the promoted variants will not continue to form without any restriction. Self-coordination exists between variants in the system, which relaxes part of the elastic distortion energy. Therefore, other variants can be formed to balance the elastic distortion energy.

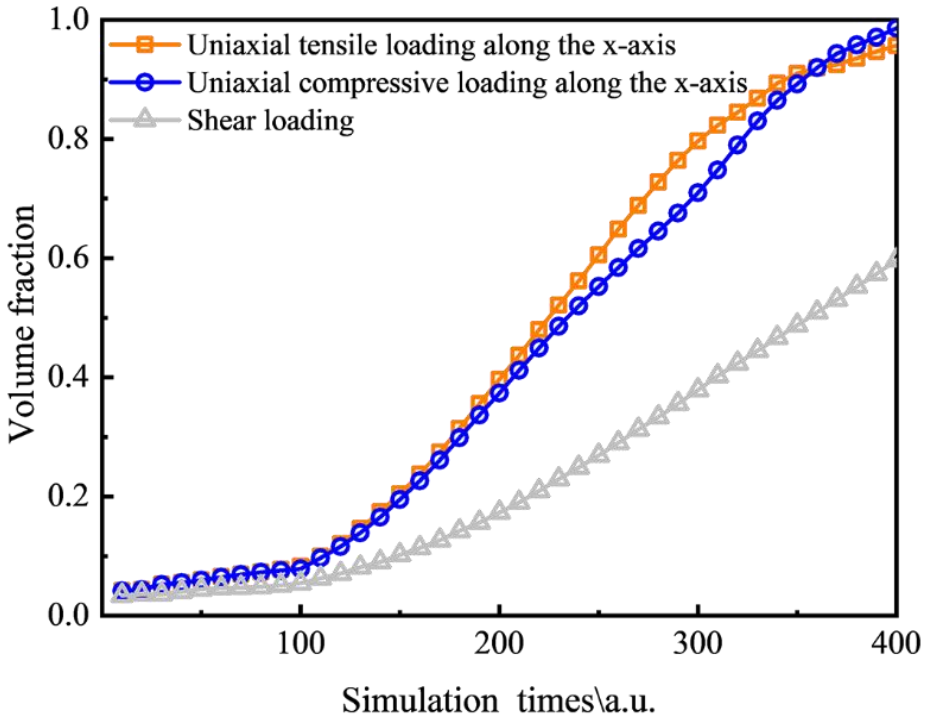

Figure 4. The kinetic curves of martensite transformation for different loading modes.

3.2. Effect of the Magnetic Field on Martensite Transformation Behaviour

In addition to the effect of the stress–strain field, the effect of the magnetic field on martensite transformation behaviour was simulated. Figure 5 shows the variation in the morphology evolution for different magnetic field intensities (0 T, 10 T, and 20 T). The results clearly reflect the difference between the effects of stress–strain and magnetic fields. For all different magnetic field intensity conditions, little preferred variant selection is observed. The fraction and final morphology of the variants under different magnetic field intensities are nearly the same. In addition, it should be noted that the time steps need for reaching the final steady state under the magnetic field and external stress field are different. In the case of the external stress field, when the time is 40 time steps (one time step equal to 10 simulation times\a.u. in this research), the transformation process tends to be stable, and the phase transformation is completed. However, in the calculation process of applying a magnetic field, the phase transformation tends to be completed when the time is 60 time steps. This will be further explained in the following kinetics results.

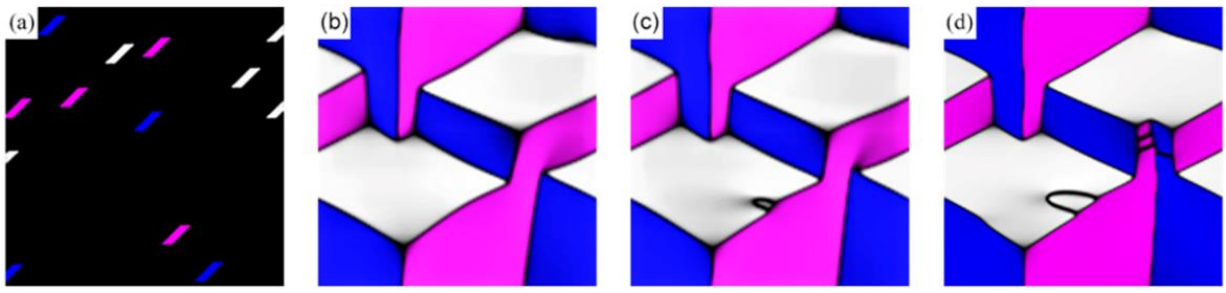

Figure 5. Variant morphology evolution for different magnetic field intensities. (**a**) Random distribution of nucleation sites, (**b**) the final steady state for 0 T magnetic field, (**c**) the final steady state for 10 T magnetic field, and (**d**) the final steady state for 20 T magnetic field.

Except for the morphological evolution, the magnetic field intensity mainly affects the kinetics of the martensite transformation. Figure 6 shows the kinetic curves of the three variants for different magnetic field intensities. Although the magnetic field intensity has

little effect on the incubation stage, a higher magnetic field intensity leads to a faster growth rate for all three variants. In addition, the degree of this influence shows little difference among the different variants. Therefore, the final number of different variants is nearly the same, indicating no obvious preferred variant selection.

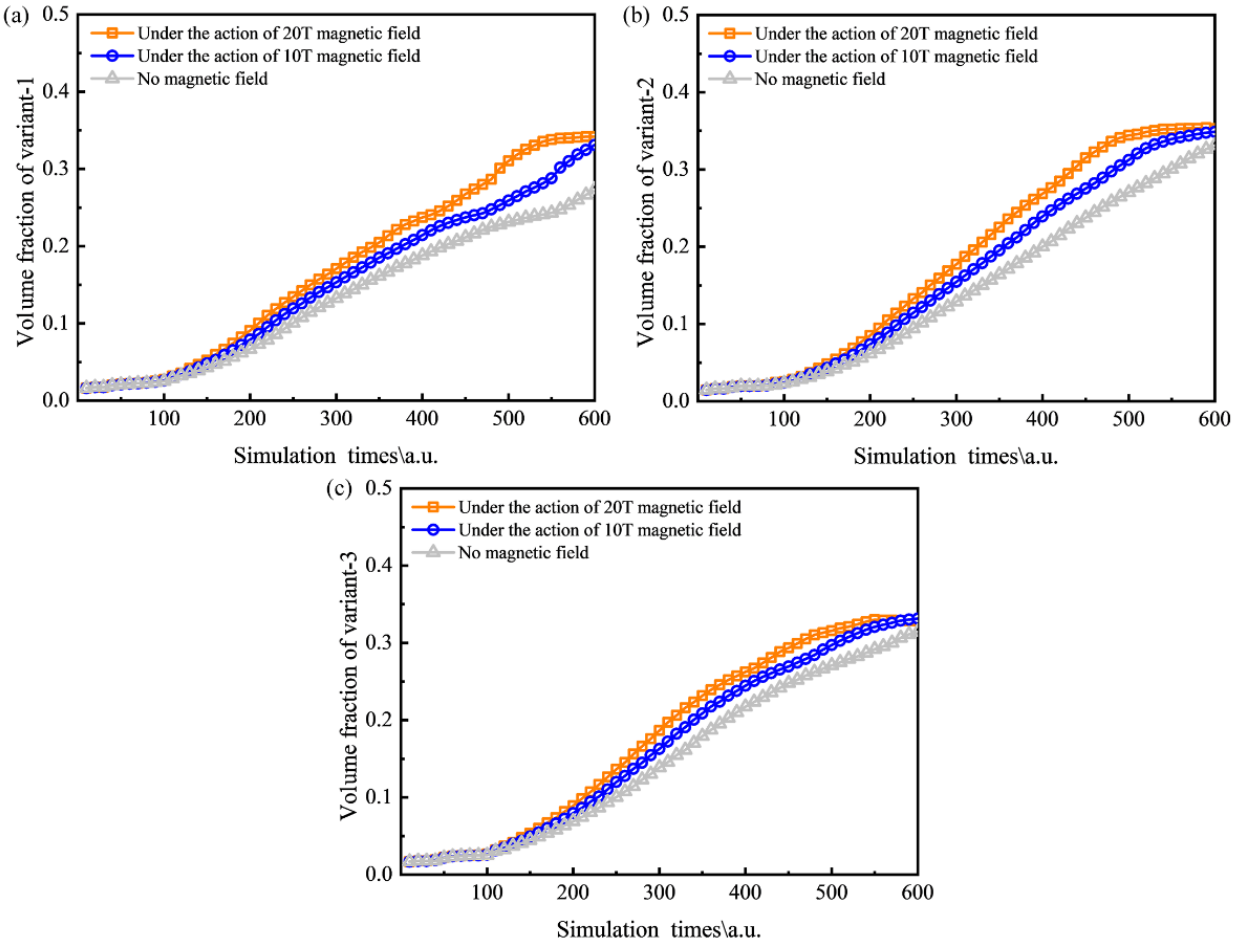

Figure 6. The kinetic curves of the three variants for different magnetic field intensities. (**a**) Variant 1, (**b**) variant 2, and (**c**) variant 3.

Figure 7 shows the kinetic curves of the martensite transformation for different magnetic field intensities. This result clearly indicates that the magnetic field can accelerate isothermal martensitic transformation in stainless steel. With an increase in the magnetic field intensity, the martensite transformation process gradually accelerates. Because the effect of the magnetic field is based on the increase in nucleation activation energy, the magnetic field intensity affects the kinetics, not the morphology or variant selection of martensite, as expected. This viewpoint is also supported by previous experimental research by Yuan et al. [21]. In addition, by comparing Figures 4 and 7, the effect of the stress–strain field on martensite transformation kinetics is much more significant than that of the magnetic field. In summary, the simulation results of this study show that different external fields can affect martensite characteristics. Stress–strain fields, especially uniaxial tension and compression conditions, can significantly accelerate martensite transformation; however, they can cause obvious preferred variant selection. Instead, the magnetic field is a gentler way to accelerate the martensite transformation without preferred variant selection. These simulation results can provide guidance for tailoring martensite characteristics using external fields.

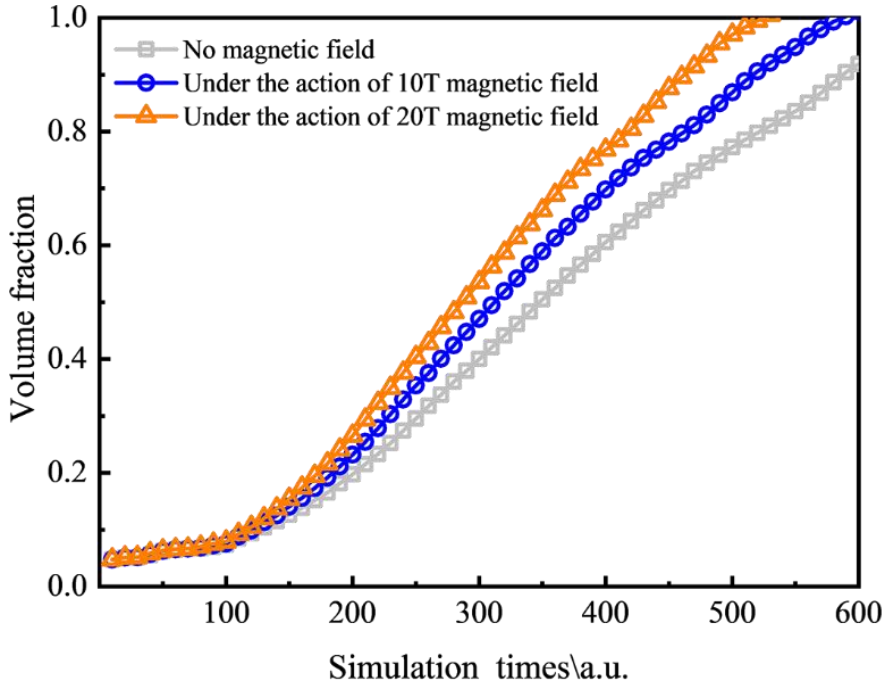

Figure 7. The kinetic curves of martensite transformation for different magnetic field intensities.

4. Discussion

All the simulation results of this study show that different external fields can affect martensite characteristics. Stress–strain fields, especially uniaxial tension and compression conditions, can significantly accelerate martensite transformation; however, they can cause obvious preferred variant selection. Instead, the magnetic field is a gentler way to accelerate the martensite transformation without preferred variant selection. These simulation results can provide qualitative guidance for tailoring martensite characteristics using external fields.

It should be further noted that the simulation of the martensite transformation in this research is based on the theory of three Bain strain groups. Only three variants form in this simulation, which is different from the actual state of 24 variants. This hypothesis provides both advantages and disadvantages for this research. Considering the advantages, the theory of Bain strain groups is a basic and generic mechanism for the martensite transformation, so it can greatly improve the generality of this model. The regular conclusions obtained from this simulation can be used for qualitative guidance on various alloy design. However, as mentioned above, three variants are different from the actual experimental results of 24 variants, which means that the results of this research are only qualitative rules. It cannot be quantitatively consistent with the experimental results of a special alloy system. So, if further improvement is needed for quantitative guidance on alloy design for a special composition system, modification is needed to replace the theory of Bain strain groups to the 24 variants with the Kurdjumov–Sachs orientational relationship as in Ahluwalia et al.'s work [33].

5. Conclusions

A phase-field model was built to simulate the effect of different external fields on martensite transformation behaviour, which can provide qualitative guidance for microstructure tailoring in advanced steels.

(1) Both stress–strain and magnetic fields can accelerate the martensite transformation process and increase the volume fraction of martensite by introducing an additional driving force.

(2) Both uniaxial tension and compression conditions can significantly promote the martensite transformation by significantly increasing the martensite growth rate. However, an obviously preferred variant selection is also observed.
(3) If a relatively large amount of martensite with an unknown preferred variant selection is needed, shearing is probably a better choice because this mode has a relatively balanced stress distribution in different directions compared to those of uniaxial tension and compression conditions.
(4) In addition, if the demand for martensite is relatively small, the magnetic field, which has a relatively low phase transition rate, can be considered. This gentler method is conducive to a more precise control of the martensite volume fraction.

Author Contributions: Writing—original draft preparation, C.W.; data curation, writing, reviewing, and editing, J.Y. and M.H.; formal analysis and supervision, C.W. All authors have read and agreed to the published version of the manuscript.

Funding: This study was financially supported by the National Natural Science Foundation of China (Grant No. 52171109, Grant No. U1808208).

Institutional Review Board Statement: Not applicable.

Informed Consent Statement: Not applicable.

Data Availability Statement: The data presented in this study are available upon request from the corresponding author.

Conflicts of Interest: The authors declare no potential conflict of interest.

References

1. Wang, M.; Huang, M.X. Abnormal TRIP effect on the work hardening behavior of a quenching and partitioning steel at high strain rate. *Acta Mater.* **2020**, *188*, 551–559. [CrossRef]
2. Josep Roa, J.; Suarez, S.; Guitar, A.; Fargas, G.; Mateo, A. Geometrically necessary dislocations on plastic deformation of polycrystalline TRIP steel. *Crystals* **2019**, *9*, 289. [CrossRef]
3. Qayyum, F.; Guk, S.; Schmidtchen, M.; Kawalla, R.; Prahl, U. Modeling the local deformation and transformation behavior of cast X8CrMnNi16-6-6 TRIP steel and 10% Mg-PSZ composite using a continuum mechanics-based crystal plasticity model. *Crystals* **2020**, *10*, 221. [CrossRef]
4. Schroeder, C.; Wendler, M.; Kreschel, T.; Volkova, O.; Weiss, A. Development of a stainless austenitic nitrogen-alloyed CrMnNiMo spring steel. *Crystals* **2019**, *9*, 456. [CrossRef]
5. Yu, D.; Chen, Y.; Huang, L.; An, K. Tracing phase transformation and lattice evolution in a TRIP sheet steel under high-temperature annealing by real-time in situ neutron diffraction. *Crystals* **2018**, *8*, 360. [CrossRef]
6. Zhao, Y.; Zhao, P.; Li, W.; Kou, S.; Jiang, J.; Mao, X.; Yang, Z. The Microalloying effect of Ce on the mechanical properties of medium entropy bulk metallic glass composites. *Crystals* **2019**, *9*, 483. [CrossRef]
7. Li, Y.; Chen, S.; Wang, C.; San Martin, D.; Xu, W. Modeling retained austenite in Q&P steels accounting for the bainitic transformation and correction of its mismatch on optimal conditions. *Acta Mater.* **2020**, *188*, 528–538. [CrossRef]
8. Seo, E.J.; Cho, L.; De Cooman, B.C. Kinetics of the partitioning of carbon and substitutional alloying elements during quenching and partitioning (Q&P) processing of medium Mn steel. *Acta Mater.* **2016**, *107*, 354–365. [CrossRef]
9. Seo, E.J.; Cho, L.; Estrin, Y.; De Cooman, B.C. Microstructure-mechanical properties relationships for quenching and partitioning (Q&P) processed steel. *Acta Mater.* **2016**, *113*, 124–139. [CrossRef]
10. Kim, J.H.; Park, W.S.; Chun, M.S.; Kim, J.J.; Bae, J.H.; Kim, M.H.; Lee, J.M. Effect of pre-straining on low-temperature mechanical behavior of AISI 304L. *Mater. Sci. Eng. A* **2012**, *543*, 50–57. [CrossRef]
11. Lee, J.M.; Seul-Kee, K. Numerical simulation of membrane of LNG insulation system using user defined material subroutine. *J. Comput. Struct. Eng. Inst. Korea* **2014**, *27*, 265–272. [CrossRef]
12. Kamali, H.; Xie, H.; Bi, H.; Chang, E.; Xu, H.; Yu, H.; Jiang, Z. Deformation mechanism and texture evolution of a low-Ni Cr–Mn–N austenitic stainless steel under bending deformation. *Mater. Sci. Eng. A* **2021**, *804*, 140724. [CrossRef]
13. Kim, H.; Park, J.; Ha, Y.; Kim, W.; Sohn, S.S.; Kim, H.S.; Lee, B.J.; Kim, N.J.; Lee, S. Dynamic tension–compression asymmetry of martensitic transformation in austenitic Fe–(0.4, 1.0)C–18Mn steels for cryogenic applications. *Acta Mater.* **2015**, *96*, 37–46. [CrossRef]
14. Nakada, N.; Ito, H.; Matsuoka, Y.; Tsuchiyama, T.; Takaki, S. Deformation-induced martensitic transformation behavior in cold-rolled and cold-drawn type 316 stainless steels. *Acta Mater.* **2010**, *58*, 895–903. [CrossRef]
15. Sohrabi, M.J.; Naghizadeh, M.; Mirzadeh, H. Deformation-induced martensite in austenitic stainless steels: A review. *Arch. Civ. Mech. Eng.* **2020**, *20*, 124. [CrossRef]

16. Iwamoto, T.; Tsuta, T.; Tomita, Y. Investigation on deformation mode dependence of strain-induced martensitic transformation in trip steels and modelling of transformation kinetics. *Int. J. Mech. Sci.* **1998**, *40*, 173–182. [CrossRef]
17. Xu, Y.; Zhang, S.; Song, H.; Cheng, M.; Zhang, H. The enhancement of transformation induced plasticity effect on austenitic stainless steels by cyclic tensile loading and unloading. *Mater. Lett.* **2011**, *65*, 1545–1547. [CrossRef]
18. Yi, S.; Gao, S.; Shen, L.X. Fracture toughening mechanism of shape memory alloys under mixed-mode loading due to martensite transformation. *Inter. J. Solids Struct.* **2001**, *38*, 4463–4476. [CrossRef]
19. Wang, J.; Wang, C.; Huang, M.; Hu, J.; Xu, W. The effects and mechanisms of pre-deformation with low strain on temperature-induced martensitic transformation. *Acta Metal. Sin.* **2021**, *57*, 575–585. [CrossRef]
20. Suru, M.G.; Morosanu, C.; Bujoreanu, L.G. Variation tendencies of shape memory alloys surface relief as a function of training-cycling parameters. *J. Optoelectron. Adv. M* **2014**, *16*, 394–400. [CrossRef]
21. Jiahua, Y.; Qiuhong, Z.; Jinliang, W.; Chenchong, W.; Wei, X. Synergistic effect of magnetic field and grain size on martensite nucleation and variant selection. *Acta Metall. Sin.* **2022**. [CrossRef]
22. Karaca, H.E.; Basaran, B.; Karaman, I.; Chumlyakov, Y.I. Stress-induced martensite to austenite phase transformation in Ni2MnGa magnetic shape memory alloys. *Smart Mater. Struct.* **2012**, *21*, 045011. [CrossRef]
23. Schastlivtsev, V.M.; Kaletina, Y.V.; Fokina, E.A.; Yakovleva, I.L. Electron-microscopic examination of martensite crystals nucleated in the N24G4 steel under the action of a DC magnetic field. *Fizika Metallov i Metallovedenie* **2003**, *95*, 68–77.
24. Fei, H.; Hedstrom, P.; Hoglund, L.; Borgenstam, A. A Thermodynamic-based model to predict the fraction of martensite in steels. *Metall. Mater. Trans. A* **2016**, *47A*, 4404–4410. [CrossRef]
25. Lee, S.J.; Van Tyne, C.J. A kinetics model for martensite transformation in plain carbon and low-alloyed steels. *Metall. Mater. Trans. A* **2012**, *43A*, 422–427. [CrossRef]
26. Mathevon, A.; Massardier, V.; Fabregue, D.; Ollat, M.; Rocabois, P.; Perez, M. Thermodynamic-based model coupled with phase transformation simulation to predict the ms temperature in the case of two-phase steel. *Metall. Mater. Trans. A* **2022**, *53*, 1674–1681. [CrossRef]
27. Artemev, A.; Khachaturyan, A.G. The phase field model and computer simulation of martensitic transformation under applied stresses. *Mater. Sci. Forum* **2000**, *327–328*, 347–350. [CrossRef]
28. Malik, A.; Amberg, G.; Borgenstam, A.; Ågren, J. Effect of external loading on the martensitic transformation—A phase field study. *Acta Mater.* **2013**, *61*, 7868–7880. [CrossRef]
29. Ghosh, G.; Olson, G.B. Kinetics of F.C.C. → B.C.C. heterogeneous martensitic nucleation—I. The critical driving force for athermal nucleation. *Acta Metall.* **1994**, *42*, 3361–3370. [CrossRef]
30. Ghosh, G.; Olson, G.B. Kinetics of F.c.c. → b.c.c. heterogeneous martensitic nucleation—II. Thermal activation. *Acta Metall.* **1994**, *42*, 3371–3379. [CrossRef]
31. Li, C.; Gao, J.; Zhang, D.; Chen, Z.; Han, X. Influence of material parameters on 2D-martensitic transformation based on the phase-field finite-element method. *Metall. Res. Technol.* **2019**, *116*, 614. [CrossRef]
32. Yeddu, H.K.; Lookman, T.; Saxena, A. The simultaneous occurrence of martensitic transformation and reversion of martensite. *Mater. Sci. Eng. A* **2014**, *594*, 48–51. [CrossRef]
33. Ahluwalia, R.; Mikula, J.; Laskowski, R.; Quek, S.S. Phase field simulation of martensitic-transformation-induced plasticity in steel. *Phys. Rev. Mater.* **2020**, *4*, 103607. [CrossRef]
34. Basaka, A.; Levitas, V.I. Matrix-precipitate interface-induced martensitic transformation within nanoscale phase field approach: Effect of energy and dimensionless interface width. *Acta Mater.* **2020**, *189*, 255–265. [CrossRef]
35. Kundin, J.; Raab, D.; Emmerich, H. A phase-field model for incoherent martensitic transformations including plastic accommodation processes in the austenite. *J. Mech. Phys. Solids* **2021**, *59*, 2082–2102. [CrossRef]
36. Song, P.; Ji, Y.; Chen, L.; Liu, W.; Zhang, C.; Chen, L.Q.; Yang, Z. Phase-field simulation of austenite growth behavior: Insights into the austenite memory phenomenon. *Comp. Mater. Sci.* **2016**, *117*, 139–150. [CrossRef]
37. Shchyglo, O.; Du, G.; Engels, J.K.; Steinbach, I. Phase-field simulation of martensite microstructure in low-carbon steel. *Acta Mater.* **2019**, *175*, 415–425. [CrossRef]
38. San Martín, D.; Aarts, K.W.P.; Rivera-Díaz-del-Castillo, P.E.J.; van Dijk, N.H.; Brück, E.; van der Zwaag, S. Isothermal martensitic transformation in a 12Cr–9Ni–4Mo–2Cu stainless steel in applied magnetic fields. *J. Magn. Magn. Mater.* **2008**, *320*, 1722–1728. [CrossRef]
39. Martin, D.S.; van Dijk, N.H.; Brück, E.; van der Zwaag, S. The isothermal martensite formation in a maraging steel: A magnetic study. *Mater. Sci. Eng. A* **2008**, *481–482*, 757–761. [CrossRef]
40. Malik, A.; Yeddu, H.K.; Amberg, G.; Borgenstam, A.; Ågren, J. Three dimensional elasto-plastic phase field simulation of martensitic transformation in polycrystal. *Mater. Sci. Eng. A* **2012**, *556*, 221–232. [CrossRef]
41. Tsuchida, N.; Tomota, Y. A micromechanic modeling for transformation induced plasticity in steels. *Mater. Sci. Eng. A* **2000**, *285*, 345–352. [CrossRef]